

# Large Cross-Phase Modulations at the Few-Photon Level

Zi-Yu Liu,<sup>1</sup> Yi-Hsin Chen,<sup>2</sup> Yen-Chun Chen,<sup>1</sup> Hsiang-Yu Lo,<sup>1</sup>

Pin-Ju Tsai,<sup>1</sup> Ite A. Yu,<sup>2†</sup> Ying-Cheng Chen,<sup>3</sup> and Yong-Fan Chen,<sup>1\*</sup>

<sup>1</sup>*Department of Physics, National Cheng Kung University, Tainan 70101, Taiwan*

<sup>2</sup>*Department of Physics and Frontier Research Center on Fundamental and Applied Sciences of Matters, National Tsing Hua University, Hsinchu 30013, Taiwan*

<sup>3</sup>*Institute of Atomic and Molecular Sciences, Academia Sinica, Taipei 10617, Taiwan*

(Dated: July 5, 2016)

We demonstrate an efficient cross-phase modulation (XPM) based on a closed-loop double- $\Lambda$  system. The property of the double- $\Lambda$  medium can be controlled by changing the phases of the applied optical fields. This phase-dependent XPM scheme can achieve large phase modulations at low-light intensities without requiring cavities or tightly focusing of laser beams. With this scheme, we observe a  $\pi$ -level phase shift with two pulses both consisting of 8 photons in cold rubidium atoms. Such novel scheme provides a simple route to generate strong interactions between photons and may have potential applications in all-optical quantum signal processing.

The realization of large cross-phase modulations (XPM) at low-light intensities, ultimately at the single-photon level, is an important but challenging task in quantum information science [1–3]. To reach this goal, one often requires high-finesse cavities to enhance nonlinear interactions between photons [4, 5]. However, cavity-based experiments require many compromises such as balancing cavity bandwidth and light-matter coupling strength, which remain technical difficulties. Another promising approach for generating strong photon-photon interaction is electromagnetically induced transparency (EIT) [6–8], but according to the theoretical predictions by Harris and coworkers, the cross-phase shift of the EIT-based Kerr medium in free space has an upper limit of order 0.1 radians at the single-photon level [9]. To date, EIT-based XPM on the order of micro-radians per photon has been observed in cold atoms [10, 11] and Rb-filled fiber system [12]. In recent years, to overcome this upper limit there have been many theoretical proposals and experimental studies on this subject including double slow-light schemes [13, 14], stationary light schemes [15, 16], cavity EIT schemes [17, 18], or Rydberg EIT schemes [19–24]. Very recently, two research teams have overcome this upper limit and observed single-photon cross-phase shifts of  $\pi/3$  and  $\pi$  by using cavity EIT [25] and Rydberg EIT [26], respectively. This is a great progress toward implementing a photon-photon gate.

Here we report an experimental observation of a novel XPM scheme based on a phase-dependent double- $\Lambda$  system. With this scheme, we observe a large cross-phase shift of  $3.6 \pm 1.0$  radians induced by a light pulse containing around 8 photons in cold rubidium atoms. This XPM scheme does not require cavities or Rydberg atoms, which provides a simple route to generate strong interactions between photons and obtain large cross-phase shifts per photon.

In the present study, we investigate a closed-loop double- $\Lambda$  XPM in a laser-cooled  $^{87}\text{Rb}$  atomic system,

as depicted in Fig. 1(a). Cold atomic gas with an optical depth of approximately 50 is produced in a dark spontaneous-force optical trap (SPOT) [27]. A strong coupling field ( $\Omega_c$  denotes its Rabi frequency) drives the  $|2\rangle \leftrightarrow |3\rangle$  transition to create a transparent medium for a weak probe pulse ( $\Omega_p$ ,  $|1\rangle \leftrightarrow |3\rangle$ ) through quantum interference. The coupling and probe fields form the first  $\Lambda$ -type EIT system. The second  $\Lambda$ -type EIT system is created by a strong driving field ( $\Omega_d$ ,  $|2\rangle \leftrightarrow |4\rangle$ ) and a weak signal pulse ( $\Omega_s$ ,  $|1\rangle \leftrightarrow |4\rangle$ ). In the experiment, the coupling and probe fields are right circularly polarized ( $\sigma+$ ) while the driving and signal fields are left circularly polarized ( $\sigma-$ ). The four laser fields drive the  $D_2$ -line transition of the  $^{87}\text{Rb}$  atoms to form the closed-loop double- $\Lambda$  EIT system, as shown in Fig. 1(a).

A schematic diagram of the experimental setup is shown in Fig. 1(b). The probe and signal fields are produced using a single diode laser (DL1); the coupling and driving fields are produced using another diode laser (DL2). DL2 is directly injection locked using an external cavity diode laser (ECDL, TOPTICA DL 100) with a laser linewidth of around 1 MHz. One beam from the ECDL is sent through a 6.8-GHz electro-optic modulator (EOM, New Focus 4851). DL1 is injection locked by an intermediate laser seeded with the high-frequency sideband of the EOM output. The above arrangement is capable of completely eliminating the influence of the carrier of the EOM output on DL1. The probe beam is overlapped with the signal beam on a polarization beam splitter (PBS2), and then sent to a single-mode fiber (SMF) to obtain the optimal spatial mode-matching. The  $e^{-2}$  diameters of the probe (signal) and coupling (driving) beams are 0.2 mm and 3 mm, respectively. These two beams propagate at an angle of around  $1^\circ$ . All of the laser fields are switched on and off via acousto-optic modulators (AOMs). We utilize AOM1 to control the widths of the probe and signal pulses. The coupling and driving fields are switched on and off via AOM4 [see Fig. 1(b)]. The experimental data are detected by a pho-

tomultiplier tube module (PMT, Hamamatsu H6780-20 and C9663) with a conversion gain of around  $9 \times 10^7$  V/W, and then recorded using an oscilloscope (Agilent MSO6034A) throughout the experiment. The number of photons of the few-photon pulses (probe and signal pulses) are also checked by a single-photon counting module (SPCM, Perkin-Elmer SPCM-AQR-13).

When conducting the phase-dependent double- $\Lambda$  experiment, an electro-optic phase modulator (EPM, Thorlabs EO-PM-NR-C1) is applied to vary the phase of the coupling field ( $\Omega_c$ ). Furthermore, to stabilize the relative phase of the four laser fields, two main setups are utilized in this experiment. (i) The optical paths of the probe and signal (coupling and driving) fields are arranged in the configuration of a Sagnac-like interferometer to reduce the path fluctuations between these two beams, as shown in Fig. 1(b). (ii) AOM2 and AOM3 are driven by the same RF generator through an RF power splitter (Mini-Circuits ZMSC-2-1+).

We utilize a sensitive beat-note interferometer to measure the cross-phase shift of the weak probe pulse. The probe beam is first split into the transmitted and reflected beams by PBS1 in order to establish the beat-note interferometer [see Fig. 1(b)]. The transmitted beam passes through the AOM1, which has a driving frequency of 80 MHz, to generate a first-order beam for the probe pulse and then recombines with the reflected beam from the PBS1 on a beam splitter (BS). One beam from the BS is called the reference beat notes, which is directly received by a photo detector (PD, New Focus 1801). The other beam, corresponding to the probe beat notes, is detected by a PMT after propagating through the double- $\Lambda$  medium. The phase shift of the probe pulse is measured by directly comparing the reference and probe beat notes. In this experiment, only the phase shift within  $1 \mu\text{s}$  of the end of the probe pulse is measured in order to acquire the steady-state results. The probe transmission is simultaneously obtained from the amplitude of the probe beat notes. The experimental setup and details of the beat-note interferometer can be found in Ref. [28].

To theoretically analyze the behavior of the probe and signal pulses propagating in the double- $\Lambda$  EIT medium, we use the Maxwell-Schrödinger equations below:

$$\frac{\partial \Omega_p}{\partial z} + \frac{1}{c} \frac{\partial \Omega_p}{\partial t} = i \frac{\alpha_p \gamma_{31}}{2L} \rho_{31}, \quad (1)$$

$$\frac{\partial \Omega_s}{\partial z} + \frac{1}{c} \frac{\partial \Omega_s}{\partial t} = i \frac{\alpha_s \gamma_{41}}{2L} \rho_{41}, \quad (2)$$

where  $\Omega_p = |\Omega_p|e^{i\phi_p}$  and  $\Omega_s = |\Omega_s|e^{i\phi_s}$  are the Rabi frequencies of the probe and signal pulses, respectively.  $\phi_p$  ( $\phi_s$ ) describes the phase information carried by the probe (signal) pulse.  $\rho_{31}$  ( $\rho_{41}$ ) is the slowly-varying amplitude of the optical coherence of the probe (signal) transition.  $\alpha_p = n\sigma_{13}L$  ( $\alpha_s = n\sigma_{14}L$ ) represents the optical depth of

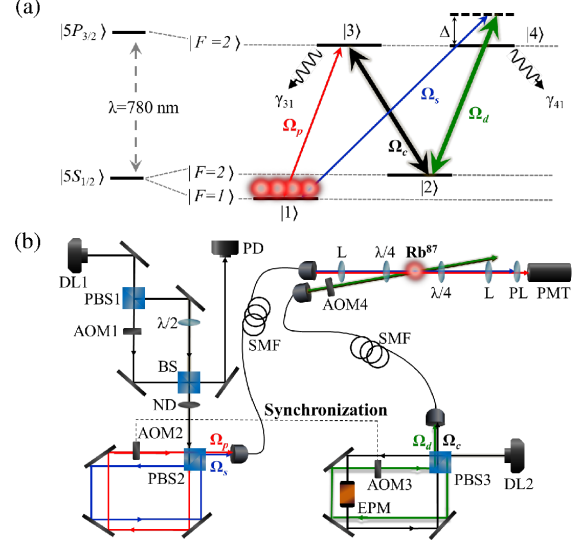


FIG. 1: Energy level scheme and experimental apparatus. (a) Energy levels of  $^{87}\text{Rb}$   $D_2$ -line transition for the double- $\Lambda$  experiment. Signal detuning,  $\Delta$ , is defined as  $\omega_s - \omega_{24}$ , where  $\omega_s$  and  $\omega_{24}$  are the frequencies of the signal field and the  $|2\rangle \leftrightarrow |4\rangle$  transition, respectively. (b) Schematic diagram of the experimental setup. DL, diode laser; PBS, polarizing-beam splitter; AOM, acousto-optic modulator;  $\lambda/4$ , quarter-wave plate;  $\lambda/2$ , half-wave plate; PL, polarizer; ND, neutral density filter; SMF, single-mode fiber; L, Lens; PD, photo detector; EPM, electro-optic phase modulator; PMT, photo-multiplier tube.

the probe (signal) transition, where  $n$  is the number density of the atoms,  $\sigma_{13}$  ( $\sigma_{14}$ ) is the atomic absorption cross section of the probe (signal) transition, and  $L$  is the optical path length of the medium.  $\gamma_{31}$  and  $\gamma_{41}$  represent the total coherence decay rates from the  $|3\rangle$  and  $|4\rangle$  excited states, respectively. We note that the optical depths of the probe and signal transitions in this experiment are the same ( $\alpha_p = \alpha_s$ ) because  $\sigma_{13}$  is equal to  $\sigma_{14}$  by considering three degenerate Zeeman sublevels, as shown in Fig. 1(a).

In the case where the probe and signal fields are very weak (i.e.,  $\rho_{11} \simeq 1$ ), the optical Bloch equations of the slowly-varying amplitudes of the density-matrix elements are given by:

$$\frac{d}{dt} \rho_{41} = \frac{i}{2} \Omega_s + \frac{i}{2} \Omega_d \rho_{21} + \left( i\Delta - \frac{\gamma_{41}}{2} \right) \rho_{41}, \quad (3)$$

$$\frac{d}{dt} \rho_{31} = \frac{i}{2} \Omega_p + \frac{i}{2} \Omega_c \rho_{21} - \frac{\gamma_{31}}{2} \rho_{31}, \quad (4)$$

$$\frac{d}{dt} \rho_{21} = \frac{i}{2} \Omega_c^* \rho_{31} + \frac{i}{2} \Omega_d^* \rho_{41} - \frac{\gamma_{21}}{2} \rho_{21}, \quad (5)$$

where  $\Omega_c = |\Omega_c|e^{i\phi_c}$  and  $\Omega_d = |\Omega_d|e^{i\phi_d}$  are the Rabi frequencies of the coupling and driving transitions, respectively.  $\phi_c$  ( $\phi_d$ ) describes the phase information carried

by the coupling (driving) field.  $\Delta$  denotes the detuning of the signal transition [see Fig. 1(a)].  $\gamma_{21}$  represents the dephasing rate of the  $|1\rangle$  and  $|2\rangle$  ground states. Each parameter in the theoretical model is individually determined from additional experiments as follows:  $|\Omega_c|$  is determined from the separation of the two absorption peaks in the EIT spectrum.  $|\Omega_d|$  is determined from the EIT-based photon-switching effect [29].  $\alpha_p$  is derived from the delay time of the slow light pulse [30].  $\gamma_{21}$  is  $0.0010(2)\Gamma$ , as estimated by the degree of EIT transparency.  $\Gamma = 2\pi \times 6$  MHz is the spontaneous decay rate of the excited states.  $\gamma_{31}$  and  $\gamma_{41}$  are both  $1.25(2)\Gamma$ , contributed mostly by the spontaneous decay rate and laser linewidth, as obtained from the spectral width of the one-photon absorption. Assume  $\gamma_{21} = 0$ ,  $\gamma_{31} = \gamma_{41}$  and  $\alpha_p = \alpha_s = \alpha$ , the steady-state solutions of Eqs. (1)–(5) for the probe and signal fields are:

$$\Omega_p(\alpha) = \frac{1}{|\Omega|^2} \left[ |\Omega_c|^2 \Omega_p(0) + \Omega_c \Omega_d^* \Omega_s(0) \right] + \frac{1}{|\Omega|^2} \left[ |\Omega_d|^2 \Omega_p(0) - \Omega_c \Omega_d^* \Omega_s(0) \right] e^{-i\frac{\alpha}{2\xi}}, \quad (6)$$

$$\Omega_s(\alpha) = \frac{1}{|\Omega|^2} \left[ |\Omega_d|^2 \Omega_s(0) + \Omega_d \Omega_c^* \Omega_p(0) \right] + \frac{1}{|\Omega|^2} \left[ |\Omega_c|^2 \Omega_s(0) - \Omega_d \Omega_c^* \Omega_p(0) \right] e^{-i\frac{\alpha}{2\xi}}, \quad (7)$$

where  $|\Omega|^2 = |\Omega_c|^2 + |\Omega_d|^2$ ,  $\xi = i + 2\frac{|\Omega_c|^2 \Delta}{|\Omega|^2 \gamma_{31}}$ . The terms  $\Omega_p(0)$  and  $\Omega_s(0)$  represent the incident probe and signal fields, respectively. Under the conditions of  $|\Omega_c| = |\Omega_d|$  and  $|\Omega_p(0)| = |\Omega_s(0)|$ , we obtain a simple steady-state solutions for the probe and signal fields as follows:

$$\frac{\Omega_p(\alpha)}{\Omega_p(0)} = \frac{1}{2} \left[ 1 + e^{-i\phi_r} + (1 - e^{-i\phi_r}) e^{-i\frac{\alpha}{2\xi}} \right], \quad (8)$$

$$\frac{\Omega_s(\alpha)}{\Omega_s(0)} = \frac{1}{2} \left[ 1 + e^{i\phi_r} + (1 - e^{i\phi_r}) e^{-i\frac{\alpha}{2\xi}} \right]. \quad (9)$$

where the relative phase of the four laser fields,  $\phi_r$ , is defined as  $\phi_p - \phi_c + \phi_d - \phi_s$ . According to Eqs. (8) and (9), when  $\Delta = 0$  and  $\phi_r = 0$ , the double- $\Lambda$  medium becomes completely transparent for both the probe and the signal fields. On the other hand, when  $\phi_r = \pi$ , the medium becomes opaque and has maximum attenuation for both the probe and the signal fields. This phase-dependent double- $\Lambda$  system with  $\Delta = 0$  can be applied in all-optical switching, as previously described [31]. Here we focus on demonstrating large phase modulations at low-light intensities with this scheme. Of note, the matched propagation of a pair of slow light pulses in the double- $\Lambda$  medium has been theoretically discussed in Ref. [32]. Recently, the closed-loop double- $\Lambda$  system can be engineered to achieve broadly tunable light shifts at low-light intensities has also been theoretically studied in Ref. [33].

We first measure the transmission of a probe pulse propagating through a three-level  $\Lambda$ -type EIT medium.

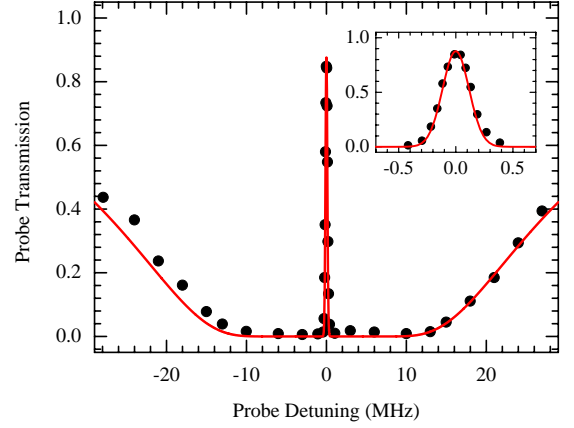


FIG. 2: Observed EIT transmission versus probe field detuning. The black circles and red line represent the measurement data and theoretical curve, respectively. The inset shows the EIT transmission window. Probe detuning is defined as  $\omega_p - \omega_{13}$ , where  $\omega_p$  and  $\omega_{13}$  are the frequencies of the probe field and the  $|1\rangle \leftrightarrow |3\rangle$  transition, respectively. The parameters for the theoretical curve are  $\alpha_p = 52$ ,  $|\Omega_c| = 0.7\Gamma$ ,  $\gamma_{21} = 0.001\Gamma$ , and  $\gamma_{31} = \gamma_{41} = 1.25\Gamma$ .

After all of the lasers and magnetic fields of the dark SPOT are turned off and the coupling field ( $\Omega_c$ ) is switched on for  $100 \mu\text{s}$ , the  $10\text{-}\mu\text{s}$  probe square pulse is switched on to perform the measurement. The experiment is conducted at a repetition rate of  $100$  Hz. The input power of the probe pulse is set to  $1$  nW in the EIT experiment. The Rabi frequency of the coupling transition,  $|\Omega_c|$ , is  $0.7\Gamma$ , corresponding to the coupling laser power of around  $0.5$  mW. Figure 2 shows the probe transmission as a function of probe detuning. The inset shows the EIT transmission window. The measurement data (circles) are in good agreement with the theoretical curve (red line). The theoretical curve is plotted using the EIT theoretical expression in Ref. [28].

Next, we perform the double- $\Lambda$  experiment in the pulsed regime. Figure 3 shows a typical experimental data, where  $\alpha_p = 46$ ,  $\Delta = 13\Gamma$ ,  $|\Omega_c| = |\Omega_d| = 0.7\Gamma$ , and the input powers of both the probe and the signal pulses are set to  $1$  nW, corresponding to  $|\Omega_p(0)| = |\Omega_s(0)| \approx 0.016\Gamma$  (i.e.,  $|\Omega_{p(s)}(0)| \ll |\Omega_{c(d)}|$ ). Here the widths of both the probe and signal pulses are set to  $10 \mu\text{s}$ . We utilized the EPM to vary the relative phase  $\phi_r$  [see Fig. 1(b)]. The relative phase  $\phi_r$  is set to  $1.5$  radians in Fig. 3(a) and  $4.5$  radians in Fig. 3(b). The solid and dashed lines represent the experimental data and theoretical curves, respectively. The theoretical curves are plotted by numerically solving Eqs. (1)–(5). The black (green) lines are the input probe (signal) pulses, and the blue (red) lines are the transmitted probe (signal) pulses. The group-velocity mismatch of the transmitted probe and signal pulses in Fig. 3 is due to  $\Delta \neq 0$ . The experimental data also show that the power of the

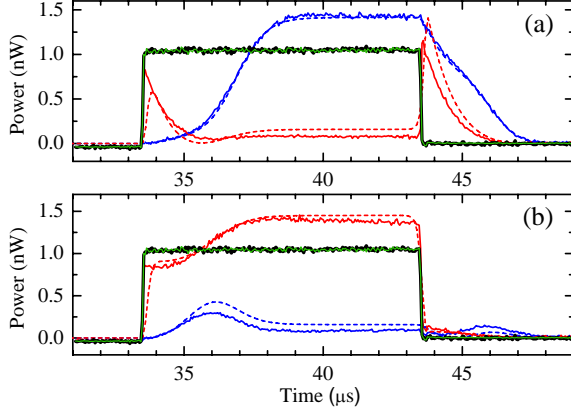


FIG. 3: Phase-dependent double- $\Lambda$  experiment in the pulsed regime. The solid and dashed lines represent the experimental data and theoretical curves, respectively. The black (green) lines are the input probe (signal) pulses; the blue (red) are the transmitted probe (signal) pulses. The parameters for the theoretical curves (dashed lines) are  $\alpha_p = 46$ ,  $|\Omega_c| = |\Omega_d| = 0.7\Gamma$ ,  $\Delta = 13\Gamma$ ,  $\gamma_{21} = 0.001\Gamma$ ,  $\gamma_{31} = \gamma_{41} = 1.25\Gamma$ . (a) the relative phase  $\phi_r = 1.5$  rad. (b)  $\phi_r = 4.5$  rad. The peak powers of both the probe and signal pulses are 1 nW, corresponding to around 40,000 photons per pulse.

transmitted light exceeds its input power in the double- $\Lambda$  system. This light-amplification phenomenon is caused by of the coherent light transfer between two N-type FWM processes ( $|1\rangle \rightarrow |3\rangle \rightarrow |2\rangle \rightarrow |4\rangle \rightarrow |1\rangle$  and  $|1\rangle \rightarrow |4\rangle \rightarrow |2\rangle \rightarrow |3\rangle \rightarrow |1\rangle$ ) [34]. For more detailed discussions for the coherent light amplification can be found in the Supplemental Material [35].

Figure 4 shows the experimental data of the double- $\Lambda$ -based XPM at low-light levels. The experimental parameters are the same as those in Fig. 3 except for the optical depth ( $\alpha_p = 50$ ). We first perform the double- $\Lambda$  experiment where the input powers of both the probe and the signal pulses are set to 10 pW, corresponding to around 400 photons per pulse. Figure 4(a) and 4(b) show the experimental data of the dependence of the probe transmission and phase shift on the relative phase  $\phi_r$ , respectively, which are in agreement with the theoretical curves. We subsequently perform the double- $\Lambda$  experiment at the few-photon level. The input powers of both the probe and the signal pulses in Figs. 4(c) and 4(e) are reduced to around 1 and 0.2 pW, corresponding to around 40 and 8 photons, respectively. Circles (squares) represent the experimental data of the probe transmission (phase shift). The blue (red) lines are the theoretical curves of the probe transmission (phase shift). Throughout the experiment, the statistical error bar is evaluated using 6 samples. Each sample is averaged 4096, 16384 and 32768 times for the measurement with 400, 40, and 8 incident photons, respectively. All error bars in this paper represent a statistical uncertainty of one standard deviation. We note that under the conditions

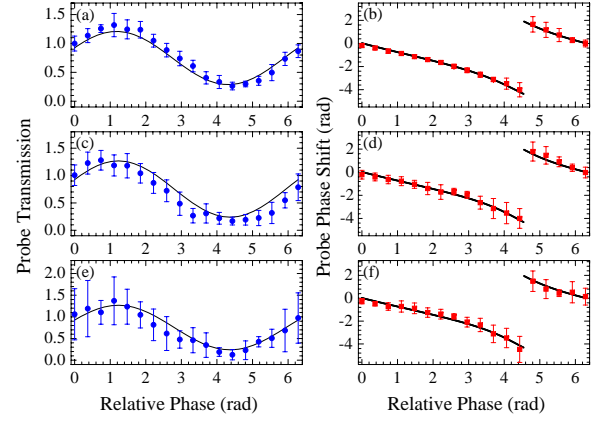


FIG. 4: Phase modulations at the few-photon level. Dependence of the transmission and the phase shift of the probe pulse on the relative phase  $\phi_r$ . The numbers of both the probe and the signal photons are around 400 in (a) and (b); 40 in (c) and (d); 8 in (e) and (f). Circles (squares) represent the transmission (phase shift) of the probe pulse. The blue and red lines are the theoretical curves of the probe transmission and phase shift, respectively. The parameters for the theoretical curves are  $\alpha_p = 50$ ,  $|\Omega_c| = |\Omega_d| = 0.7\Gamma$ ,  $\Delta = 13\Gamma$ ,  $\gamma_{21} = 0.001\Gamma$ ,  $\gamma_{31} = \gamma_{41} = 1.25\Gamma$ .

of  $|\Omega_c| = |\Omega_d|$  and  $|\Omega_p(0)| = |\Omega_s(0)|$ , the probe transmission and phase modulation after propagating through the double- $\Lambda$  medium are the same according to Eqs. (8) and (9). A detailed theoretical analysis can be found in the Supplemental Material [35].

As the number of the probe and signal photons decreases, the error bars of the measurement data become large due to smaller signal-to-noise ratios, as shown in Fig. 4. Although the data in Fig. 4(f) possess a large amount of phase noise of around 1 radians, the measured values are still valid considering the considerable phase shift. For instance, in Fig. 4(f), a maximum phase shift of  $-4.5 \pm 0.9$  radians is measured when the relative phase  $\phi_r$  is set to 4.4 radians. When the signal pulse is absent, we also measure the probe phase shift of  $-0.9 \pm 0.1$  radians which is consistent with the theoretical predictions. Hence, we conclude that a cross-phase shift of  $3.6 \pm 1.0$  radians induced by a light pulse containing around 8 photons has been realized with this scheme. So far we do not perform the experiment using few-photon pulses containing less than 8 photons because the long-term instability of our experimental system prevents us from improving the signal-to-noise ratios by collecting more data. In principle, this phase-dependent XPM scheme can reach the goal of  $\pi$  phase modulation per photon if one can prepare two phase-coherent single-photon pulses to be as the probe and signal pulses.

In conclusion, we have demonstrated an efficient XPM based on a closed-loop double- $\Lambda$  system. The property of the double- $\Lambda$  medium can be controlled by changing the phases of the applied optical fields. This phase-

dependent XPM scheme can achieve large phase modulations at low-light intensities without requiring cavities or Rydberg atoms. We have observed a cross-phase shift of  $3.6 \pm 1.0$  radians induced by a light pulse containing 8 photons in cold  $^{87}\text{Rb}$  atoms with this scheme. Such novel scheme provides a simple route to generate strong interaction between photons, and may have potential applications in all-optical quantum signal processing.

### ACKNOWLEDGEMENTS

We acknowledge Hao-Chung Chen, You-Lin Chuang and Ray-Kuang Lee for helpful discussions and Jun-Jie Wu for experimental assistance. This work was supported by the National Science Council of Taiwan under grants numbers 103-2119-M-006-018 and 104-2119-M-006-002. This work was done under a collaboration project (Science Vanguard Research Program of MOST) with Ite A. Yu as the project leader and Ying-Cheng Chen and Yong-Fan Chen as the subproject leaders. Correspondence of the project contents can be addressed to Ite A. Yu; correspondence and requests for material of this work can be addressed to Yong-Fan Chen. We also acknowledge the support from NCTS of Taiwan.

---

\* Electronic address: yfchen@mail.ncku.edu.tw; † Email address: yu@phys.nthu.edu.tw

- [1] D. Bouwmeester, A. Ekert, and A. Zeilinger, *The Physics of Quantum Information* (Springer, New York, 2000).
- [2] M. A. Nielsen and I. L. Chuang, *Quantum Computation and Quantum Information* (Cambridge University Press, Cambridge, 2000).
- [3] N. Imoto, H. A. Haus, and Y. Yamamoto, Phys. Rev. A **32**, 2287 (1985).
- [4] Q. A. Turchette, C. J. Hood, W. Lange, H. Mabuchi, and H. J. Kimble, Phys. Rev. Lett. **75**, 4710 (1995).
- [5] I. Fushman, D. Englund, A. Faraon, N. Stoltz, P. Petroff, and J. Vučković, Science **320**, 769 (2008).
- [6] S. E. Harris, Phys. Today **50**, 36 (1997).
- [7] M. D. Lukin, Rev. Mod. Phys. **75**, 457 (2003).
- [8] M. Fleischhauer, A. Imamoglu, and J. P. Marangos, Rev. Mod. Phys. **77**, 633 (2005).
- [9] S. E. Harris and L. V. Hau, Phys. Rev. Lett. **82**, 4611 (1999).
- [10] H.-Y. Lo, Y.-C. Chen, P.-C. Su, H.-C. Chen, J.-X. Chen, Y.-C. Chen, I. A. Yu, and Y.-F. Chen, Phys. Rev. A **83**, 041804(R) (2011).
- [11] A. Feizpour, M. Hallaji, G. Dmochowski, and A. M. Steinberg, Nat. Phys. **11**, 905 (2015).
- [12] V. Venkataraman, K. Saha, and L. Gaeta, Nat. Photonics. **7**, 138 (2012).
- [13] M. D. Lukin and A. Imamoglu, Phys. Rev. Lett. **84**, 1419 (2000).
- [14] B.-W. Shiao, M.-C. Wu, C.-C. Lin, and Y.-C. Chen, Phys. Rev. Lett. **106**, 193006 (2011).
- [15] M. Bajcsy, A. S. Zibrov, and M. D. Lukin, Nature **426**, 638 (2003).
- [16] Y.-H. Chen, M.-J. Lee, W. Hung, Y.-C. Chen, Y.-F. Chen, and I. A. Yu, Phys. Rev. Lett. **108**, 173603 (2012).
- [17] M. Mücke, E. Figueroa, J. Bochmann, C. Hahn, K. Murr, S. Ritter, C. J. Villas-Boas, and G. Rempe, Nature **465**, 755 (2010).
- [18] Y. Zhu, Opt. Lett. **35**, 303 (2010).
- [19] I. Friedler, D. Petrosyan, M. Fleischhauer, and G. Kurizki, Phys. Rev. A **72**, 043803 (2005).
- [20] A. K. Mohapatra, T. R. Jackson, and C. S. Adams, Phys. Rev. Lett. **98**, 113003 (2007).
- [21] J. D. Pritchard, D. Maxwell, A. Gauguier, K. J. Weatherill, M. P. A. Jones, and C. S. Adams, Phys. Rev. Lett. **105**, 193603 (2010).
- [22] A. V. Gorshkov, J. Otterbach, M. Fleischhauer, T. Pohl, M. D. Lukin, Phys. Rev. Lett. **107**, 133602 (2011).
- [23] S. Baur, D. Tiarks, G. Rempe, S. Dür, Phys. Rev. Lett. **112**, 073901 (2014).
- [24] H. Gorniaczyk, C. Tresp, J. Schmidt, H. Fedder, S. Hofferberth, Phys. Rev. Lett. **113**, 053601 (2014).
- [25] K. M. Beck, M. Hosseini, Y. Duan, and V. Vuletić, arXiv:1512.02166
- [26] D. Tiarks, S. Schmidt, G. Rempe, and S. Dür, Science Advances **2**, 4 (2016).
- [27] W. Ketterle, K. B. Davis, M. A. Joffe, A. Martin, and D. E. Pritchard, Phys. Rev. Lett. **70**, 2253 (1993).
- [28] H.-Y. Lo, P.-C. Su, Y.-W. Cheng, P.-I. Wu, and Y.-F. Chen, Opt. Express **18**, 18498 (2010).
- [29] Y.-F. Chen, Z.-H. Tsai, Y.-C. Liu, and I. A. Yu, Opt. Lett. **30**, 3207 (2005).
- [30] L. V. Hau, S. E. Harris, Z. Dutton, and C. H. Behroozi, Nature **397**, 594 (1999).
- [31] H. Kang, G. Hernandez, J. Zhang, and Y. Zhu, Phys. Rev. A **73**, 011802(R) (2006).
- [32] L. Deng and M. G. Payne, Phys. Rev. A **71**, 011803(R) (2005).
- [33] M. Artoni and A. Zavatta, Phys. Rev. Lett. **115**, 113005 (2015).
- [34] C.-K. Chiu, Y.-H. Chen, Y.-C. Chen, I. A. Yu, Y.-C. Chen, and Y.-F. Chen, Phys. Rev. A **89**, 023839 (2014).
- [35] See Supplemental Material for a detailed discussion.

# Supplemental Material for "Large Cross-Phase Modulations at the Few-Photon Level"

(Dated: July 5, 2016)

## I. THEORETICAL MODEL

We consider an atomic medium consisting of double- $\Lambda$ -type four-level transitions with two metastable ground states ( $|1\rangle$  and  $|2\rangle$ ) and two excited states ( $|3\rangle$  and  $|4\rangle$ ), as shown in Fig. S1. Weak probe (with the Rabi frequency  $\Omega_p$ ) and strong coupling ( $\Omega_c$ ) fields form the first electromagnetically induced transparency (EIT) system, and weak signal ( $\Omega_s$ ) and strong driving ( $\Omega_d$ ) fields constitute the second EIT system. For an individual EIT system,  $\Omega_c$  ( $\Omega_d$ ) manipulates the transmission of  $\Omega_p$  ( $\Omega_s$ ) through an optical dense medium and causes the  $\Omega_p$  ( $\Omega_s$ ) to become transparent because of destructive quantum interference. When the conditions  $|\Omega_c| \gg |\Omega_p|$  and  $|\Omega_d| \gg |\Omega_s|$  are satisfied, all the atoms remain in the ground state  $|1\rangle$  and the contribution of the probe and signal fields can be treated as a perturbation in the derivation of the following equations. The double- $\Lambda$  EIT medium can induce two N-type four-wave mixing (FWM) processes: first,  $|1\rangle \rightarrow |3\rangle \rightarrow |2\rangle \rightarrow |4\rangle \rightarrow |1\rangle$ , generating the signal field; and second,  $|1\rangle \rightarrow |4\rangle \rightarrow |2\rangle \rightarrow |3\rangle \rightarrow |1\rangle$ , generating the probe field [S1]. Thus, the energy as well as the phases of the probe and signal fields are coherently transferred via these two FWM paths. We begin deriving equations from the interaction Hamiltonian between atoms and optical fields and the equations of motion of the density matrix operators. The steady-state analytical solutions for the double- $\Lambda$  EIT system can be obtained by solving the first-order optical Bloch equations (OBEs) of the density matrix operators and the Maxwell-Schrödinger equations (MSEs) of the probe and signal pulses as follows:

$$\frac{d}{dt}\rho_{41} = \frac{i}{2}\Omega_s + \frac{i}{2}\Omega_d\rho_{21} + \left(i\Delta - \frac{\gamma_{41}}{2}\right)\rho_{41}, \quad (\text{S1})$$

$$\frac{d}{dt}\rho_{31} = \frac{i}{2}\Omega_p + \frac{i}{2}\Omega_c\rho_{21} - \frac{\gamma_{31}}{2}\rho_{31}, \quad (\text{S2})$$

$$\frac{d}{dt}\rho_{21} = \frac{i}{2}\Omega_c^*\rho_{31} + \frac{i}{2}\Omega_d^*\rho_{41} - \frac{\gamma_{21}}{2}\rho_{21}, \quad (\text{S3})$$

$$\frac{\partial\Omega_p}{\partial z} + \frac{1}{c}\frac{\partial\Omega_p}{\partial t} = i\frac{\alpha_p\gamma_{31}}{2L}\rho_{31}, \quad (\text{S4})$$

$$\frac{\partial\Omega_s}{\partial z} + \frac{1}{c}\frac{\partial\Omega_s}{\partial t} = i\frac{\alpha_s\gamma_{41}}{2L}\rho_{41}, \quad (\text{S5})$$

where  $\alpha_{p(s)}$  represents the optical depth of the probe (signal) field transition;  $\rho_{ij}$  is the slowly varying amplitude of the coherence between states  $|i\rangle$  and  $|j\rangle$ ;  $\gamma_{31(41)} \equiv \Gamma_{3(4)} + \gamma_{3(4)}$  is the total coherence decay rate of the excited state  $|3\rangle$  ( $|4\rangle$ ), where  $\Gamma_{3(4)}$  and  $\gamma_{3(4)}$  represent the total spontaneous decay rate of the excited state  $|3\rangle$  ( $|4\rangle$ ) and the energy-conserving dephasing rate, respectively [S2];  $\gamma_{21}$  is the dephasing rate of the coherence between the ground states  $|1\rangle$  and  $|2\rangle$ ;  $L$  is the optical path length of the medium; and  $\Delta$  denotes the detuning of the signal field transition.

For simplicity, we assume  $\alpha_p = \alpha_s \equiv \alpha$ ,  $\gamma_{31} = \gamma_{41} \equiv \Gamma$ , and  $\gamma_{21} = 0$ . With the time-derivative terms being zero, we derive the steady-state solutions by solving the first-order OBEs [Eqs. (S1)–(S3)] as follows:

$$\begin{aligned} \rho_{21} &= \frac{\Omega_p\Omega_c^*(2\Delta + i\Gamma) + \Omega_s\Omega_d^*(i\Gamma)}{D}, \\ \rho_{31} &= \frac{\Omega_p|\Omega_d|^2 - \Omega_s\Omega_c\Omega_d^*}{D}, \\ \rho_{41} &= \frac{\Omega_s|\Omega_c|^2 - \Omega_p\Omega_c^*\Omega_d}{D}, \end{aligned} \quad (\text{S6})$$

where  $D = -[i\Gamma|\Omega_d|^2 + (2\Delta + i\Gamma)|\Omega_c|^2]$ . By substituting Eq. (S6) into MSEs [Eqs. (S4) and (S5)] with time-derivative components being zero, we obtain the steady-state solutions for the probe and signal fields as follows:

$$\begin{aligned} \Omega_p(\alpha) &= \frac{1}{|\Omega|^2} \left[ |\Omega_c|^2 \Omega_p(0) + \Omega_c\Omega_d^*\Omega_s(0) \right] \\ &+ \frac{1}{|\Omega|^2} \left[ |\Omega_d|^2 \Omega_p(0) - \Omega_c\Omega_d^*\Omega_s(0) \right] e^{-i\frac{\alpha}{2\epsilon}}, \end{aligned} \quad (\text{S7})$$



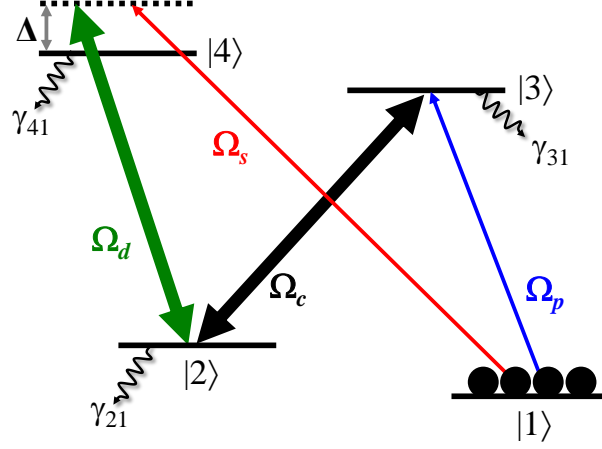


FIG. S1: Schematic energy level for a four-level double- $\Lambda$  system. States  $|1\rangle$  and  $|2\rangle$  are two metastable ground states, and states  $|3\rangle$  and  $|4\rangle$  are two excited states. Weak probe ( $\Omega_p$ ) and strong coupling ( $\Omega_c$ ) fields form the first EIT system, and weak signal ( $\Omega_s$ ) and strong driving ( $\Omega_d$ ) fields constitute the second EIT system with a detuning of  $\Delta$ . All the atoms are initially prepared in the state  $|1\rangle$ . The term  $\gamma_{31(41)}$  is the total coherence decay rate of the excited state  $|3\rangle(|4\rangle)$ . The term  $\gamma_{21}$  is the dephasing rate of the coherence between the ground states  $|1\rangle$  and  $|2\rangle$ .

$$\begin{aligned} \Omega_s(\alpha) = & \frac{1}{|\Omega|^2} \left[ |\Omega_d|^2 \Omega_s(0) + \Omega_d \Omega_c^* \Omega_p(0) \right] \\ & + \frac{1}{|\Omega|^2} \left[ |\Omega_c|^2 \Omega_s(0) - \Omega_d \Omega_c^* \Omega_p(0) \right] e^{-i\frac{\alpha}{2\xi}}, \end{aligned} \quad (\text{S8})$$

where  $|\Omega|^2 = |\Omega_c|^2 + |\Omega_d|^2$  and  $\xi = i + 2\frac{|\Omega_c|^2 \Delta}{|\Omega|^2 \Gamma}$ . The terms  $\Omega_p(0)$  and  $\Omega_s(0)$  represent the incident probe and signal fields, respectively. We then consider the phase of each laser field  $\Omega_j = |\Omega_j|e^{i\phi_j}$ , where  $j = p, s, c$ , and  $d$ . The relative phase,  $\phi_r$ , of the four optical fields is defined as  $\phi_p - \phi_c + \phi_d - \phi_s$ . Under the conditions  $|\Omega_c| = |\Omega_d|$  and  $|\Omega_p(0)| = |\Omega_s(0)|$ , we obtain the simple steady-state solutions for the probe and signal fields as follows:

$$\frac{\Omega_p(\alpha)}{\Omega_p(0)} = \frac{1}{2} \left[ 1 + e^{-i\phi_r} + (1 - e^{-i\phi_r}) e^{-i\frac{\alpha}{2\xi}} \right], \quad (\text{S9})$$

$$\frac{\Omega_s(\alpha)}{\Omega_s(0)} = \frac{1}{2} \left[ 1 + e^{i\phi_r} + (1 - e^{i\phi_r}) e^{-i\frac{\alpha}{2\xi}} \right]. \quad (\text{S10})$$

The transmission and phase shift of the transmitted probe (signal) field are  $|\Omega_{p(s)}(\alpha)/\Omega_{p(s)}(0)|^2$  and  $\tan^{-1}\{\text{Im}[\Omega_{p(s)}(\alpha)]/\text{Re}[\Omega_{p(s)}(\alpha)]\}$ , respectively. According to Eqs. (S9) and (S10), when  $\Delta = 0$  and  $\phi_r = \pi$  the double- $\Lambda$  EIT medium becomes opaque and maximally attenuates both the probe and signal fields. However, when  $\phi_r = 0$  both the probe and signal fields become completely transparent, as a result of destructive interference. This phase-dependent double- $\Lambda$  EIT scheme with  $\Delta = 0$  can be applied in low-light-level photon switching, as previously described [S3]. Theories regarding the influence of the relative phase of the applied optical fields on the light transmission when propagated through the double- $\Lambda$  medium were discussed in Ref. [S4], and the matched propagation of a pair of slow light pulses in the double- $\Lambda$  medium was studied in Ref. [S5]. Here, we focus on the effects of cross-phase modulation (XPM) and coherent light amplification based on the double- $\Lambda$  EIT scheme.

## II. RESULTS AND DISCUSSIONS

To describe the mechanism and behavior of light pulses propagating in the double- $\Lambda$  EIT medium, the influence of the signal detuning ( $\Delta$ ), the optical depth ( $\alpha$ ), and the relative phase ( $\phi_r$ ) for the optical medium are discussed in Sections II A and II B. The initial phases of the probe and signal fields ( $\phi_p$  and  $\phi_s$ ) are set to 0 in the following calculations. We draw a phase diagram to show the evolution of the phase shifts and transmission of both the probe and signal fields. The phase diagram reveals that a clear phase jump that occurs when the relative phase is varied. We discuss the phase jump in Section II C. For practical applications in optical and quantum control, an efficient

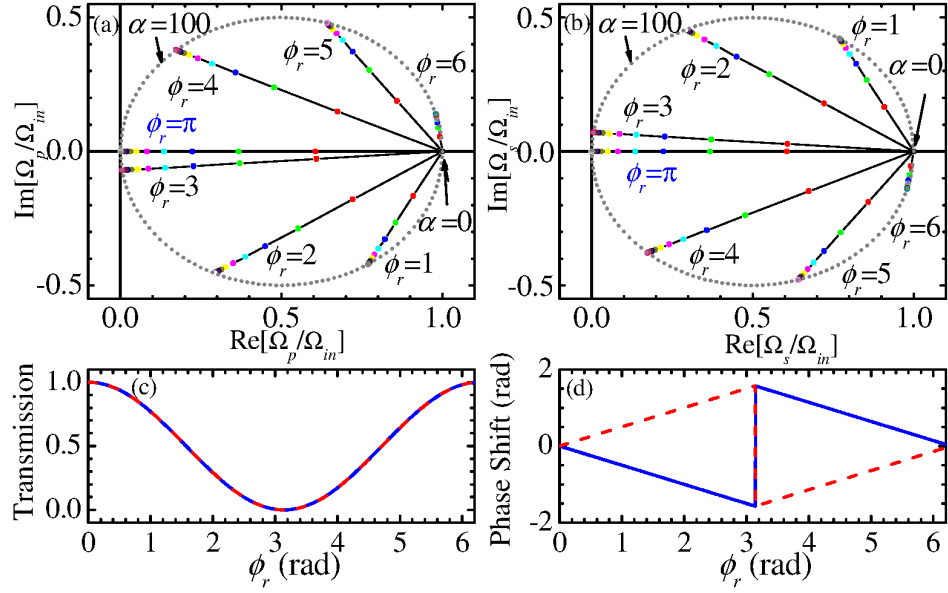


FIG. S2: Balanced double- $\Lambda$  EIT system ( $\Delta = 0$ ,  $|\Omega_c| = |\Omega_d|$ , and  $|\Omega_p(0)| = |\Omega_s(0)|$ ). (a) and (b) show phase diagrams of the probe and signal fields, respectively, plotted according to Eqs. (S9) and (S10). The optical depth,  $\alpha$ , increased from 0 to 100, clearly illustrating the phase evolutions of the light fields. The relative phases,  $\phi_r$ , are set from 1 to 6 as well as  $\pi$  in units of rad. The dotted lines show the loops of the light fields at various  $\phi_r$  values and  $\alpha = 100$ . (c) and (d) are graphs of the corresponding transmissions and phase shifts of the probe (blue solid lines) and signal fields (red dashed lines) when  $\alpha = 100$ .

XPM should satisfy a  $\pi$ -order phase shift with high transmission. We optimize the parameters for achieving this goal and provide discussions in Section II D. Finally, the effect of coherent light amplification and the dynamics of both the probe and signal pulses propagating in the double- $\Lambda$  EIT medium are presented by numerically simulating Eqs. (S1)–(S5) in Section II E. In addition, we show that the steady-state transmission obtained using the numerical simulations are consistent with those calculated using the analytical solutions [Eqs. (S9) and (S10)].

#### A. Balanced double- $\Lambda$ EIT system ( $\Delta = 0$ )

We first discuss a symmetrical double- $\Lambda$  EIT system with a signal detuning of zero ( $\Delta = 0$ ). In the case where  $|\Omega_c| = |\Omega_d|$  and  $|\Omega_p(0)| = |\Omega_s(0)|$ , the two EIT systems are identical and the two FWM paths are balanced. Figures S2(a) and S2(b) show phase diagrams of the probe and signal fields, respectively, plotted according to Eqs. (S9) and (S10). In the phase diagram, the angle between the x-axis and a line connecting the origin and data point represents the phase shift, and the square of the distance between the data point and the origin represents the transmission. To illustrate the phase evolution of both the probe and signal fields propagating through the double- $\Lambda$  EIT medium, we increase the optical depth,  $\alpha$ , from 0 to 100. The relative phase,  $\phi_r$ , is set from 1 to 6 as well as  $\pi$ , as shown in Figs. S2(a) and S2(b). The dotted lines show the loops at various  $\phi_r$  values and  $\alpha = 100$ . Figures S2(c) and S2(d) show the transmission and phase shifts of the probe (blue solid lines) and signal fields (red dashed lines). When  $\Delta = 0$ , the two FWM processes in the double- $\Lambda$  EIT system maintain a stable balance; hence, the variations of the probe and signal transmission according to the relative phase are identical [see Fig. S2(c)]. Nevertheless, the signs of the variations in the phase shifts of the probe and signal fields are opposite, as shown in Fig. S2(d). The phase shifts of the optical fields are continuous variations with  $\phi_r$  and exhibit substantial changes in sign at  $\phi_r = \pi$ . When  $\phi_r < \pi$ , the probe (signal) field acquires a negative (positive) phase shift. By contrast, when  $\phi_r > \pi$ , the probe (signal) field acquires a positive (negative) phase shift. However, when  $\phi_r = \pi$ , the phase shifts of both the probe and signal fields are always zero.

#### B. Imbalanced double- $\Lambda$ EIT system ( $\Delta \neq 0$ )

The theoretical analysis reveals that this double- $\Lambda$  EIT scheme is phase dependent. Furthermore, a large phase shift (order  $\pi$ ) of one weak probe pulse induced by another weak signal pulse can be achieved, and hence this scheme



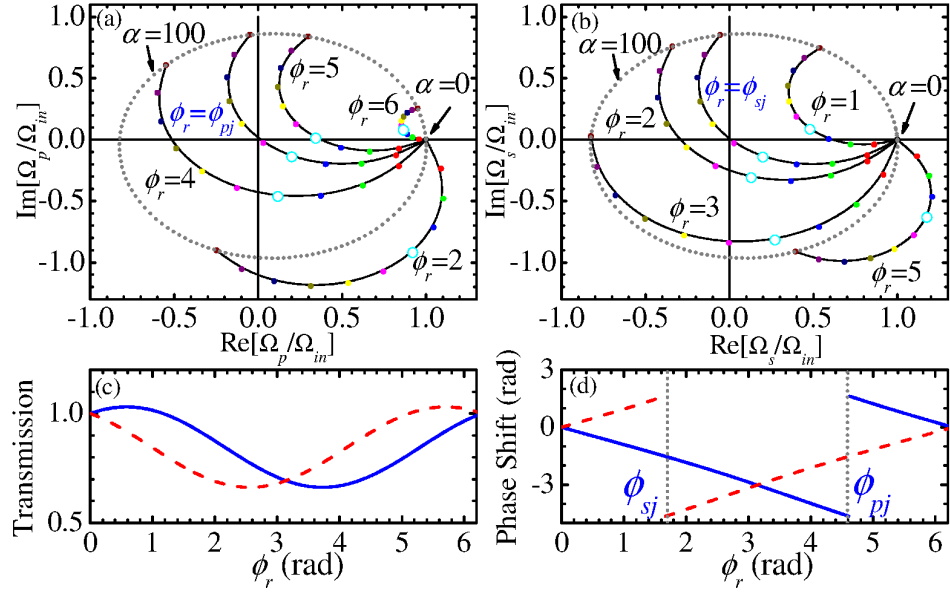


FIG. S3: Imbalanced double- $\Lambda$  EIT system ( $\Delta \neq 0$ ,  $|\Omega_c| = |\Omega_d|$ , and  $|\Omega_p(0)| = |\Omega_s(0)|$ ). (a) and (b) show phase diagrams of the probe and signal fields, respectively, plotted according to Eqs. (S9) and (S10) with  $\Delta = 16.5\Gamma$ . The values of relative phases,  $\phi_r$ , are set as shown in the plot and  $\phi_{pj} = 4.62$  and  $\phi_{sj} = 1.66$  in units of rad. (c) and (d) are graphs of the transmissions and phase shifts of the probe (blue solid lines) and signal fields (red dashed lines) when  $\alpha = 100$ .

can be applied in low-light-level XPM. However, as shown in Figs. S2(c) and S2(d), when  $\phi_r$  is close to  $\pi$ , a large phase shift ( $\approx \pi/2$ ) corresponds to low transmission ( $\approx e^{-\alpha}$ ), reducing practicality. Therefore, we consider a double- $\Lambda$  EIT system with a non-zero detuning ( $\Delta \neq 0$ ), which causes an imbalance between the two FWM processes of the double- $\Lambda$  EIT scheme.

We plotted phase diagrams with  $\Delta = 16.5\Gamma$  and  $\alpha$  ranging from 0 to 100, as shown in Fig. S3. Based on the selected parameters, a large phase shift with high light transmission can be generated, as discussed in Sec. II D. The phase diagrams show that the phase jump occurs in the probe field when  $\phi_r = \phi_{pj}$  and in the signal field when  $\phi_r = \phi_{sj}$ . Here, we define  $\phi_{pj(sj)}$  as the relative phase when the phase jump occurs in the probe (signal) field. The curve of  $\phi_r = \phi_{pj}$  or  $\phi_r = \phi_{sj}$  passing through the origin is a crucial condition for the phase jump [see Figs. S3(a) and S3(b)]. When  $\phi_r > \phi_{pj}$  (e.g.,  $\phi_r = 5$  rad), the accumulated phase shift of the transmitted probe field becomes zero at approximately  $\alpha = 40$ , as indicated by the open circles in Fig. S3(a). The probe field then exhibits a constantly increasing positive phase shift until leaving the medium ( $\alpha = 100$ ). By contrast, when  $\phi_r < \phi_{pj}$  (e.g.,  $\phi_r = 4$  rad), the probe field constantly increases negative phase shift throughout propagation. We conclude that the phase shift of the probe (signal) field as a function of  $\phi_r$  must become a phase jump when  $\phi_r = \phi_{pj}$  ( $\phi_r = \phi_{sj}$ ), as shown in Fig. S3(d).

The double- $\Lambda$  EIT scheme in which  $\Delta \neq 0$  causes an imbalance between the two FWM paths and leads to that the probe and signal fields exchange energy mutually. Hence, the energy flow causes the transmission of the probe or the signal field to be greater than unity [see Fig. S3(c)]. In addition, Figs. S3(c) and S3(d) show large phase shifts (order  $\pi$ ) with high light transmission can be achieved by using the imbalanced double- $\Lambda$  EIT scheme.

### C. Phase jump

The key factor of the phase jump depends on whether the light field disappears during the propagation process (i.e., the curve in the phase diagram passes through the origin) [see Figs. S3(a) and S3(b)]. In this section, we determine the critical optical depth ( $\alpha_c$ ) and relative phase ( $\phi_{pj}$ ) when the phase jump occurs in the probe field. The curve in the phase diagram terminates at the origin [i.e.,  $|\Omega_p(\alpha)/\Omega_p(0)|^2 = 0$  in Eq. (S9)]; hence, we obtain the following equation:

$$\cot\left(\frac{\phi_r}{2}\right)e^{-R} + \tan\left(\frac{\phi_r}{2}\right)e^R = -2\sin(I), \quad (\text{S11})$$

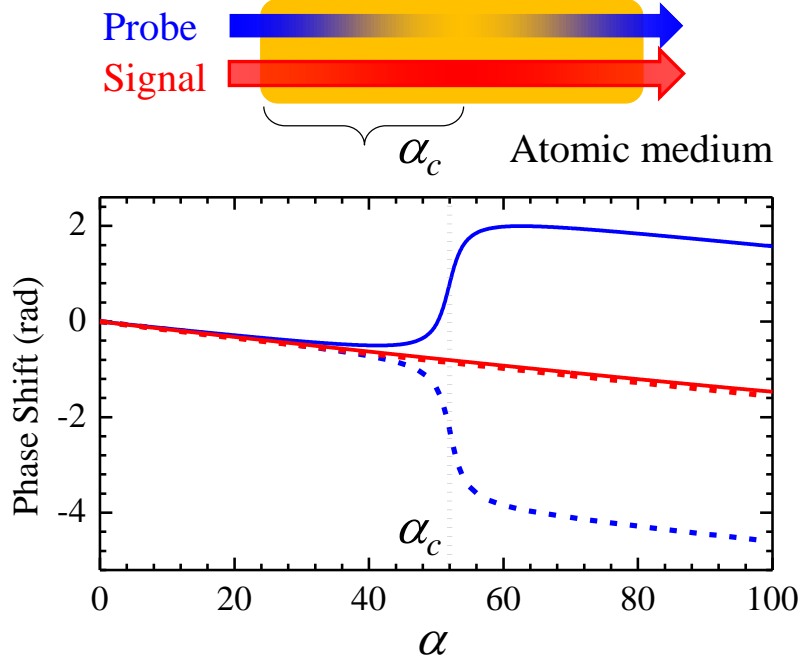


FIG. S4: The top illustration shows that the probe field exhausts its energy when the light propagates through a medium with a critical optical depth of  $\alpha_c$ . The probe field is then restored when the light field passes through the remainder of medium. The bottom figure shows the phase shifts of the probe (blue) and signal (red) fields with the relative phase right above  $\phi_{pj}$  (4.67 rad for the solid lines) and below  $\phi_{pj}$  (4.57 rad for the dashed lines), plotted according to Eqs. (S9) and (S10) with  $\Delta = 16.5\Gamma$ .

where  $R = -\frac{\alpha}{2} \frac{1}{(\Delta/\Gamma)^2 + 1}$  and  $I = \frac{\alpha}{2} \frac{\Delta/\Gamma}{(\Delta/\Gamma)^2 + 1}$ . We define  $\tan(\phi_r/2)e^R$  as  $\chi$  and simplify the above expression as  $\chi^2 + 2\sin(I)\chi + 1 = 0$ . Hence, we derive

$$\chi = -\sin(I) \pm i\cos(I). \quad (\text{S12})$$

Because  $\chi$  is a real number,  $I = n\pi/2$ , where  $n$  is an odd integer. We then obtain the analytic solutions of  $\alpha_c$  and  $\phi_{pj}$  as follows:

$$\alpha_c = n\pi \frac{(\Delta/\Gamma)^2 + 1}{\Delta/\Gamma}, \quad (\text{S13})$$

$$\phi_{pj} = 2 \tan^{-1} \left[ -\sin\left(\frac{n\pi}{2}\right) e^{\frac{n\pi}{2(\Delta/\Gamma)}} \right]. \quad (\text{S14})$$

Similarly, the relative phase of the phase jump for the signal field can be derived from Eq. (S10) as follows:

$$\phi_{sj} = 2 \tan^{-1} \left[ \sin\left(\frac{n\pi}{2}\right) e^{\frac{n\pi}{2(\Delta/\Gamma)}} \right]. \quad (\text{S15})$$

According to Eqs. (S13)-(S15) and using  $\Delta = 16.5\Gamma$  as an example, we obtain  $\alpha_c \approx 52$ ,  $\phi_{pj} \approx 4.62$  rad, and  $\phi_{sj} \approx 1.66$  rad for  $n = 1$ ; these values are consistent with the numerical results shown in Fig. S3. The phase jump occurs when the light field disappears during the propagation process. As shown in the top plot of Fig. S4, the probe field exhausts its energy when the light propagates through a medium with a critical optical depth ( $\alpha_c$ ), and the signal field gains the energy. The system is converted into an EIT-based FWM system [S1]. The probe field is then restored when it passes through the remainder of the medium. We plotted the phase shifts of the probe (blue) and signal (red) fields with the relative phase slightly above (solid lines) and below  $\phi_{pj}$  (dashed lines), as shown in the bottom plot of Fig. S4. The figure clearly illustrates the phase jump near  $\phi_{pj}$ .

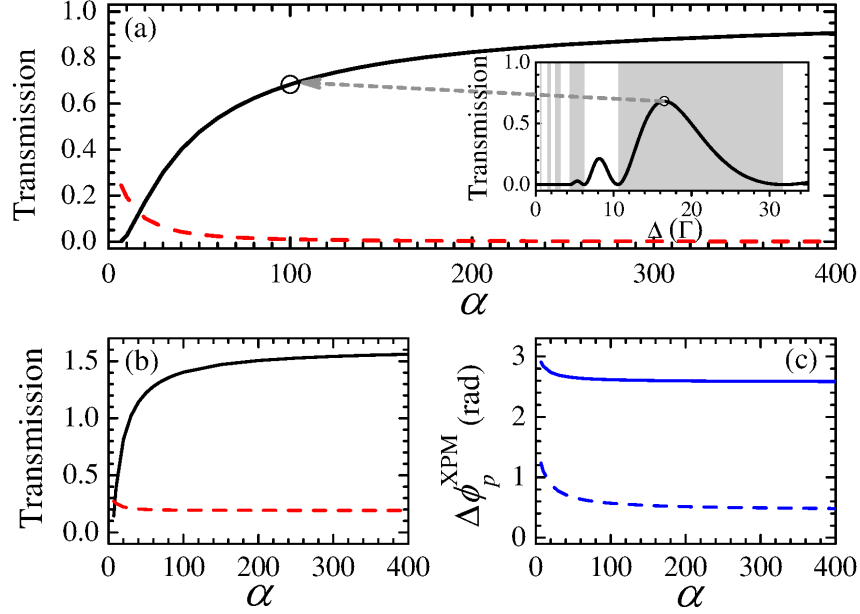


FIG. S5: (a) Inset: To achieve a  $\pi$  phase shift of the transmitted probe field ( $|\Delta\phi_p|$ ) in a double- $\Lambda$  EIT system, the probe field transmission is a function of the detuning  $\Delta$  with a fixed optical depth ( $\alpha = 100$ ). The gray zones in the figure show that the terminal point is located on the negative x-axis. A local maximum of transmission is located at approximately  $\Delta = 16.5\Gamma$ . Main plot: Using various optical depths and the corresponding optimized  $\Delta$ , we obtain the optimized probe transmission, which is a monotonous increasing function (black solid line). Without the signal field (red dashed line), the probe transmission is a monotonous decreasing function of  $\alpha$  with the corresponding  $\Delta$ . (b) Simulations similar to those shown in (a) except the phase shift of the transmitted probe field is set to  $\pi/2$ . (c) The phase modulation of the probe field with and without the signal field,  $|\Delta\phi_p^{\text{XPM}}|$ , as a function of  $\alpha$ . Blue solid and dashed lines represent the phase modulation in the simulations in (a) and (b), respectively.

#### D. Cross-phase modulation

For practicality in optical and quantum control, we discuss a  $\pi$ -order XPM with high light transmission achieved using the double- $\Lambda$  EIT scheme. To achieve a phase shift of  $\pi$ , the terminal point of the curve in the phase diagram must be located at the negative x-axis [i.e., the imaginary part of Eq. (S9) is zero and the real part is negative]. We obtain the relative phase for the  $\pi$ -phase shift of the probe field as follows:

$$\phi_r^\pi = 2 \tan^{-1} \left[ \frac{\cos(I) - e^{-R}}{\sin(I)} \right]. \quad (\text{S16})$$

In Eq. (S9),  $\phi_r$  is substituted by Eq. (S16) and we then obtain the light transmission as functions of  $\alpha$  and  $\Delta$ . We plotted the relationship between the probe field transmission and  $\Delta$  with a fixed optical depth ( $\alpha = 100$ ) in the inset of Fig. S5(a). The gray zones in the figure show that the terminal point is located on the negative x-axis. The transmission is maximal at approximately  $\Delta = 16.5\Gamma$ . Using various optical depths and the corresponding optimized  $\Delta$ , we obtain a monotonous increasing function, as indicated by the black solid line in the main plot of Fig. S5(a). A  $\pi$  phase shift with high light transmission can be achieved using the double- $\Lambda$  EIT scheme.

To apply the scheme in XPM, we compare the light transmission and phase shift with and without the signal field. In an ideal XPM technique, a weak signal pulse can modulate another weak probe pulse by a phase shift of  $\pi$  without losing energy. When no  $\Omega_s$  is applied in the proposed scheme, the probe transmission is a monotonous decreasing function of  $\alpha$  with the corresponding  $\Delta$ , as indicated by the red dashed line in Fig. S5(a). Consider the parameters  $\alpha = 100$ ,  $\Delta = 16.5\Gamma$ , and the corresponding  $\phi_r$  for example. Although the transmission can be as high as 68% when  $\Omega_s$  is present, the transmission becomes only 1% when  $\Omega_s$  is absent. The phase modulation by the signal field,  $|\Delta\phi_p^{\text{XPM}}|$ , is 2.62 rad, as indicated by the black solid line in Fig. S5(c). Hence, achieving a  $\pi$ -order XPM with high light transmission by using the double- $\Lambda$  EIT scheme remains a considerable challenge. In addition, we perform a similar simulation except the phase shift of the transmitted probe field,  $|\Delta\phi_p|$ , is set to  $\pi/2$ . In this simulation, the

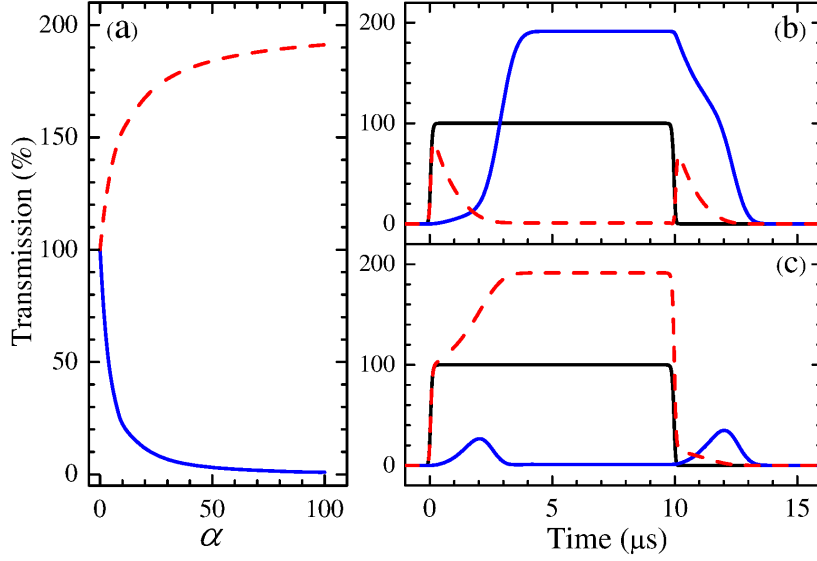


FIG. S6: (a) Optimal energy amplification for the signal field versus optical depth  $\alpha$  with the optimal detuning  $\Delta$  and relative phase  $\phi_r$  determined using numerical simulation of Eqs. (S9) and (S10). Blue solid and red dashed lines represent the transmissions of the probe and signal fields, respectively. An optical depth of 50 (100) enables achieving an amplification efficiency of approximately 84% (91%), as indicated by the red dashed line. (b) and (c) Two slow-light pulses in the double- $\Lambda$  EIT system with relative phases  $\phi_r$  of 1.53 rad and 4.76 rad to achieve maximal probe (blue solid lines) and signal transmission (red dashed lines) in (b) and (c), respectively. In this simulation,  $\alpha = 100$ ,  $\Delta = 34.2\Gamma$ ,  $\Omega_c = \Omega_d = 1\Gamma$ , and  $\gamma_{21} = 0$ . Black solid lines represent two identical incident probe and signal pulses.

real part of Eq. (S9) is zero and the terminal point in phase diagram is located on the negative y-axis. As shown in Fig. S5(b) and the blue dashed line in Fig. S5(c), the probe transmissions are 140% and 19% with and without  $\Omega_s$ , respectively, and the  $|\Delta\phi_p^{\text{XPM}}|$  is 0.57 rad when  $\alpha = 100$ .

### E. Coherent light amplification

The phase-dependent double- $\Lambda$  EIT system can coherently convert and amplify the energy of the light pulse. The two imbalanced FWM processes cause two slow-light pulses (probe and signal) to exchange energy mutually and the light transmission can be greater than unity. Numerical simulation of optimal energy amplification for the signal field (i.e., the highest signal transmission) versus optical depth with the optimal detuning and relative phase reveals that an optical depth of 50 (100) enables attaining an amplification efficiency of approximately 84% (91%), as indicated by the red dashed line in Fig. S6(a).

The dynamics of pulse-shape light propagation by numerically solving MSEs and OBEs is presented in Figs. S6(b) and S6(c). Two identical square (probe and signal) pulses are fired into the double- $\Lambda$  medium simultaneously. To clearly observe phase-dependent slow light pulses, we set  $\alpha = 100$ ,  $\Delta = 34.2\Gamma$ ,  $\Omega_c = \Omega_d = 1\Gamma$ , and  $\gamma_{21} = 0$ . The relative phases  $\phi_r$  of 1.53 rad and 4.76 rad enable achieving maximum probe (blue solid lines) and signal (red dashed lines) transmission, as shown in Figs. S6(b) and S6(c), respectively. The steady-state transmission is consistent with the results obtained by calculating Eqs. (S9) and (S10). In addition, the group velocities differ between the transmitted probe and the signal pulses because  $\Delta \neq 0$ .

- 
- [S1] C.-K. Chiu, Y.-H. Chen, Y.-C. Chen, I. A. Yu, Y.-C. Chen, and Y.-F. Chen, Phys. Rev. A **89**, 023839 (2014).
  - [S2] M. Fleischhauer, A. Imamoglu, and J. P. Marangos, Rev. Mod. Phys. **77**, 633 (2005).
  - [S3] H. Kang, G. Hernandez, J. Zhang, and Y. Zhu, Phys. Rev. A **73**, 011802(R) (2006).
  - [S4] E. A. Korsunsky and D. V. Kosachiov, Phys. Rev. A **60**, 4996 (1999).
  - [S5] L. Deng and M. G. Payne, Phys. Rev. A **71**, 011803(R) (2005).